Progress In Electromagnetics Research Letters, Vol. 113, 91–100, 2023

Flexible Irregular-Hexagonal CPW-Fed Monopole Antenna with Windmill-Shaped Fractals for Ultra-Wideband Technology

Mohamed E. Yassin[1], Yousef Hassan[1], Olaoluwa Popoola[2], Moath Alathbah[3], and Shaimaa Mohassieb[1, *]

Abstract—A novel flexible printed monopole antenna with a windmill-shaped fractal design, which is fed by co-planar waveguide (CPW) is presented in this manuscript for ultra-wideband (UWB) applications. By integrating a modified windmill-shape fractal into the conventional irregular hexagonal-patch, the antenna achieves a significantly wider impedance bandwidth extending up to 156.6% across the frequency band of 1.37–11.25 GHz. Additionally, increasing the number of the windmill-shaped fractals leads to the emergence of further resonances. The overall dimensions of the designed antenna are $50 \times 70 \times 0.2\,\text{mm}^3$, and it boasts an impressive bandwidth-dimension ratio (BDR) of 4457, showcasing exceptional efficiency in utilizing its compact size. The maximum gain reaches 4.8 dBi, while the radiation efficiency attains an impressive 98%. The modified windmill-shape fractal antenna design leverages the multifractal concept, providing monopole antennas with enhanced flexibility in controlling resonances and bandwidth. This manuscript offers a comprehensive presentation and discussion of the process used to improve the impedance bandwidth, shedding light on the antenna's exceptional performance and capabilities.

1. INTRODUCTION

In the modern era, ultra-wideband (UWB) technology operates within the 3.1–10.6 GHz frequency range, employing small pulses to transmit data with remarkably low power consumption. UWB applications enjoy a wide array of antenna options [1, 2]. Among these choices are various planar antennas with diverse feeding structures like coaxial, coplanar waveguide type, and microstrip, as well as different shapes [3]. These antennas have proven to be highly suitable for meeting the demands of UWB systems. The increasing demand for wideband antennas featuring flexibility and reduced radiation has prompted the adoption of fractal geometry. This geometric approach offers both space efficiency and self-similarity attributes. Fractal principles have emerged as a groundbreaking strategy for crafting compact UWB, wideband, and multiband antennas. The term "fractal" was initially coined by Mandelbrot in 1970s [4]. Fractals are captivating geometric patterns [5–8] distinguished by their remarkable property of self-similarity, wherein smaller components resemble the whole structure. Their prevalence in the natural world is evident, seen in intricate formations like snowflakes, the graceful patterns of peacock feathers, and the complex arrangements of broccoli. The fascination with fractals has driven researchers to explore diverse methods and techniques for generating and deriving these intricate geometric patterns. In the domain of antenna design, the incorporation of fractals has proven highly advantageous. Noteworthy fractal shapes include the Sierpinski Carpet/Gasket, Koch curve, Hilbert curve, Minkowski Island, and Meander fractal [9–14]. These antenna designs based on fractals offer unique benefits, enabling

Received 14 August 2023, Accepted 4 November 2023, Scheduled 11 November 2023

* Corresponding authors: Shaimaa Mohassieb (s.mohassieb@akhbaracademy.edu.eg).

[1] Electrical Engineering Department, Akhbar Elyom Academy, 6th of October City, Egypt. [2] James Watt School of Engineering, University of Glasgow, Glasgow, UK. [3] Electrical Engineering Department, College of Engineering, King Saud University, Riyadh, Saudi Arabia.

miniaturization by as much as 30% to 80%, all while maintaining favorable radiation characteristics. Consequently, these designs have gained widespread use across various antenna applications, addressing diverse needs such as wideband, narrowband, and multiband requirements. The fusion of fractal geometry with antenna design unlocks a realm of possibilities, fostering innovative solutions and pushing the boundaries of wireless communication technology. Fractal antennas based on flexible substrates have garnered considerable attention in recent years. These antennas utilize the fascinating properties of fractal geometry, which enables self-similarity and space-filling characteristics, making them highly versatile and efficient for various applications. The use of flexible substrates allows these antennas to conform to curved surfaces and irregular geometries, expanding their potential applications in modern communication systems and wearable devices [15, 16].

Fractal-based flexible antennas offer several advantages, including miniaturization capabilities, enhanced radiation performance, and the ability to cover a wide frequency range. As a result, they have emerged as a promising solution for wireless communication, Internet of Things (IoT) devices, and other emerging technologies. Researchers and engineers continue to explore new designs and configurations, driving innovation in the field of fractal antennas on flexible substrates, with the aim of further enhancing their performance and applications [17, 18]. Herein, we present a novel approach to enhance the bandwidth and efficiency of an antenna operating within the UWB frequency range.

Our method involves utilizing an irregular hexagonal-patch monopole antenna, fed by CPW structure, combined with five windmill fractal shapes to significantly increase the antenna's bandwidth. The proposed antenna was meticulously designed and printed on a flexible Rogers RT5880^{TM} substrate with a thickness of 0.2 mm. The paper thoroughly outlines the antenna's design, along with simulated and experimental results, providing a comprehensive assessment of the proposed UWB antenna's performance.

2. DESIGN OF THE WINDMILL-SHAPED ANTENNA

2.1. Antenna Geometry

The CST® Studio Suite 3D EM simulator (CST-MWS) is employed for the design and performance evaluation of the antenna over the desired frequency range. The antenna structure proposed in Figure 1

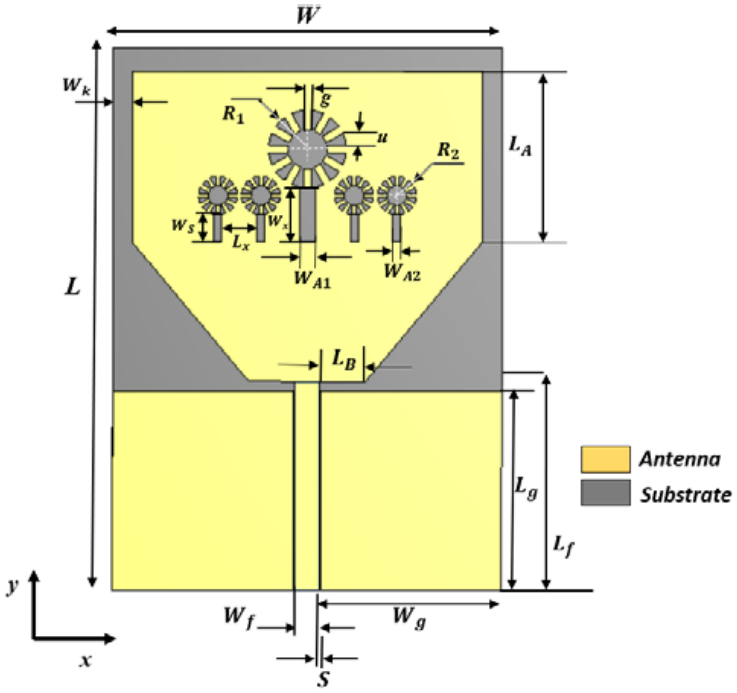

Figure 1. The dimensional parameters of the windmill-shaped fractals strip antenna's geometry.

comprises a planar irregular hexagonal monopole patch with five windmill fractal shapes, printed on the top of a flexible Rogers RT5880^{TM} substrate, characterized by a dielectric constant $\varepsilon_r = 2.2$, loss tangent "$\delta = 0.001$", and thickness 0.2 mm. The five windmill fractals are distributed into two on the right-hand side and two on the left-hand side, each scaled at a ratio of 2 : 1 from the central one.

The antenna is stimulated through a co-planar waveguide (CPW) feed line, with the CPW's length designated as L_g. The width of the central strip within the CPW is identified as W_f, while the width of each side slot is represented as S. The CPW's characteristic impedance is determined by computing values for W_f and S, employing the CPW design equations [19, 20]. For connecting the antenna to the feed line, the CPW's central strip is extended by a length of L_f. Both the antenna and CPW feed structure are printed on the same flexible substrate, Rogers RT5880^{TM}. The overall dimensions of the printed antenna are described as $L \times W \times h$, and the optimal dimensions of the proposed antenna are detailed in Table 1.

Table 1. Dimensions of the proposed antenna as presented in Figure 1.

Parameter	W	L	L_A	L_g	L_f	L_B	W_f	W_g	W_x	W_{A1}	W_{A2}	R_1	R_2	s	u	g	L_x	W_k
Value (mm)	50	70	22	25.8	27	11.4	3.2	23.2	7	2	1	2.5	1.25	0.2	1.61	1	4.5	2.5

2.2. Design Evolution

The proposed antenna design underwent a comprehensive five-step evolution, as depicted in Figure 2(a). In the initial phase, our aim was to augment the impedance bandwidth by employing a simple patch strip radiator antenna, exemplified by the geometry of Antenna #1. The $|S_{11}|$ frequency response curves displayed in Figure 2(b) reveal that the antenna achieved impedance matching over several frequency bands within the desired wideband. Moving to the second phase of the antenna design, we further refined the design by cutting the end points of the radiating strip into two triangular shapes at the bottom corners of the radiation patch. This adjustment extended the current path, resulting in an

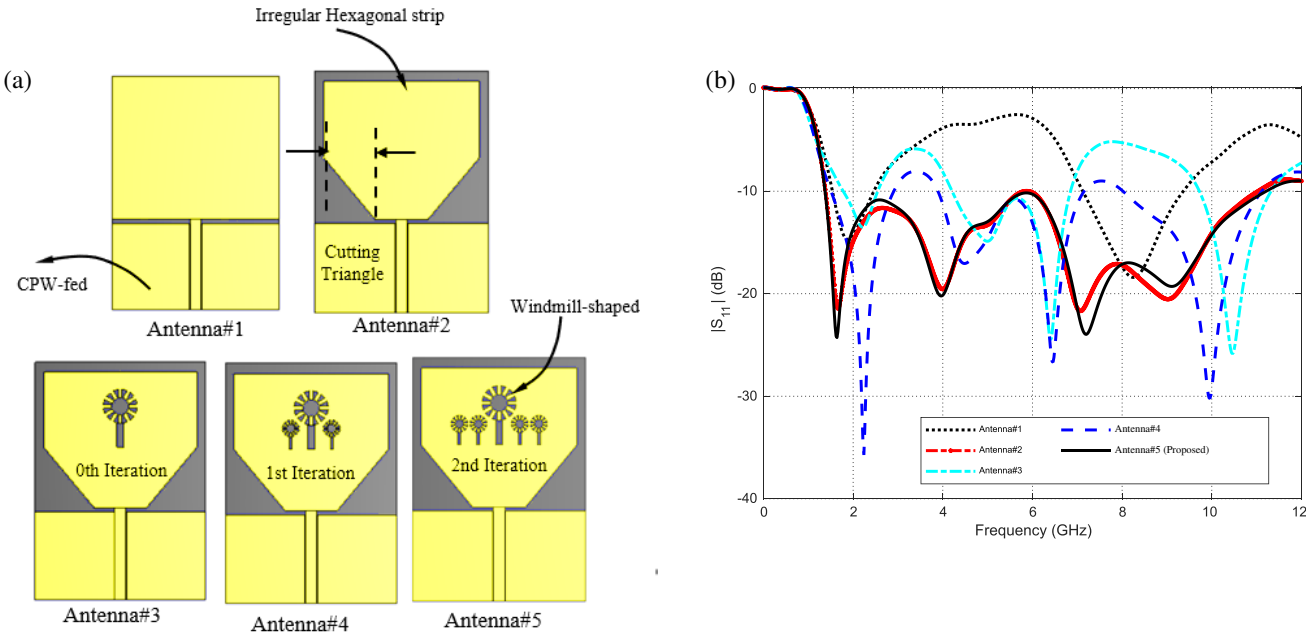

Figure 2. The development of the windmill-shaped fractals strip antenna design (a) evolution steps, and (b) the graph of the reflection coefficient $|S_{11}|$ for each design step.

irregular hexagonal shape, as embodied by Antenna #2. This alteration yielded a notable enhancement in the impedance matching bandwidth, as depicted in Figure 2(b). However, it was observed that this improvement did not necessarily guarantee uniform gain and radiation efficiency across the entire frequency band. In this stage, the gain and efficiency reached 1.4 dBi and 64.7% as illustrated in Figures 9 and 10.

Consequently, the next phase saw the development of Antenna #3, incorporating the 0th iteration of the windmill-shaped fractal design. Antenna #3 demonstrated operation within the frequency bands [1.78–2.54], [4.2–6.86], and [9.72–11.32], with respective bandwidths of 0.76, 2.66, and 1.6 GHz. The antenna structure continued to evolve with Antenna #4 (1st iteration) as part of the ongoing refinement process aimed at achieving the intended applications. In the penultimate iteration, the geometry was further modified by integrating two new windmill-shaped structures into the central one. This new configuration enabled wideband operation spanning from 3.8 to 7.18 GHz. However, it fell short of meeting the X-band technology. To further enhance antenna matching and extend the operating band to encompass the B and X bands technology [6], the design progressed to the 2nd iteration, marking the final major step in the process. This iteration culminated in the formation of Antenna #5, where the antenna was terminated with five windmill-shaped structures connected to an irregular hexagonal strip. The final design has realized the targeted UWB antenna with a gain surpassing 4.8 dBi, providing an extended operating bandwidth that comprehensively encompasses the entire frequency spectrum ranging from 1.37 to 11.25 GHz. This achievement aligns perfectly with the requisites of UWB wireless communication technology.

2.3. Effect of Bend Stresses on the Windmill-Shaped Monopole Antenna Characteristics

Due to its flexible structure, the proposed antenna maintains its high performance even when being subjected to bend strains to some extent in different directions. To investigate the effects of bend stresses on the antenna's characteristics, it is subjected to bend angle (α_T), and the corresponding frequency dependencies of the reflection coefficient $|S_{11}|$ are analyzed. The bending is applied in the transverse plane perpendicular to the feed line as illustrated in Figure 3.

Figure 4 illustrates the frequency dependence of the reflection coefficient magnitude, $|S_{11}|$, for various values of the transverse bend angle, α_T. The results demonstrate that when α_T is less than 35°, the frequency dependency of $|S_{11}|$ is minimally affected, and the impedance matching bandwidth remains relatively constant. However, for α_T values greater than or equal to 35°, $|S_{11}|$ begins to increase above −10 dB, resulting in a reduction of the impedance matching bandwidth.

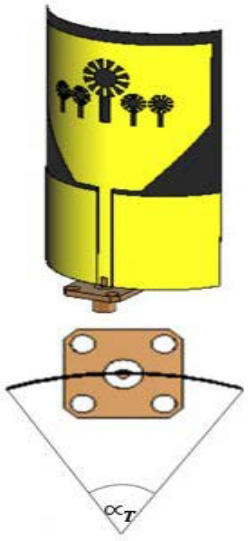

Figure 3. The proposed antenna undergoes bending stresses in the transverse plane.

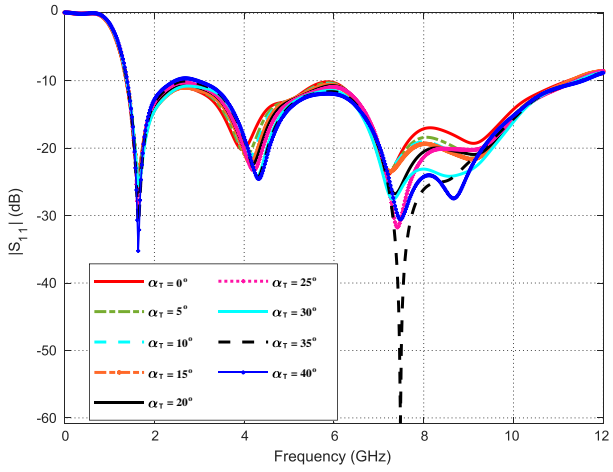

Figure 4. The reflection coefficient magnitude, $|S_{11}|$, varies with frequency for different values of the transverse bend angle, α_T.

3. EXPERIMENTAL RESULTS AND DISCUSSIONS

Following the electromagnetic simulations and determining the optimal values for the antenna design parameters listed in Table 1, a prototype is fabricated for experimental verification and measurements. The experimental results are then compared to the electromagnetic simulated ones obtained using the CST simulator. The comparison includes aspects such as the reflection coefficient, radiation pattern, gain, and radiation efficiency.

3.1. Fabrication and Measurements of Reflection Coefficient

The antenna's reflection coefficient magnitude, $|S_{11}|$, is measured by connecting it to the Rohde and Schwarz vector network analyzer (VNA) model ZVA 67, as illustrated in Figures 5(a) and 5(b) for unbent and bending angle $\alpha_T = 35°$, respectively. The frequency dependence of $|S_{11}|$, with both the experimental and simulation results showing close agreement for both unbent and bending cases as shown in Figures 6(a) and 6(b), respectively. The operating band with return losses below -10 dB spans approximately from 1.37 GHz to 11.25 GHz, consistent with both the simulated and measured results. In our study, we have designed and fabricated this flexible antenna with versatility in mind, making it adaptable for various fitting scenarios within UWB applications such as wearable UWB devices, IoT and sensor networks, consumer electronics, healthcare, and medical devices.

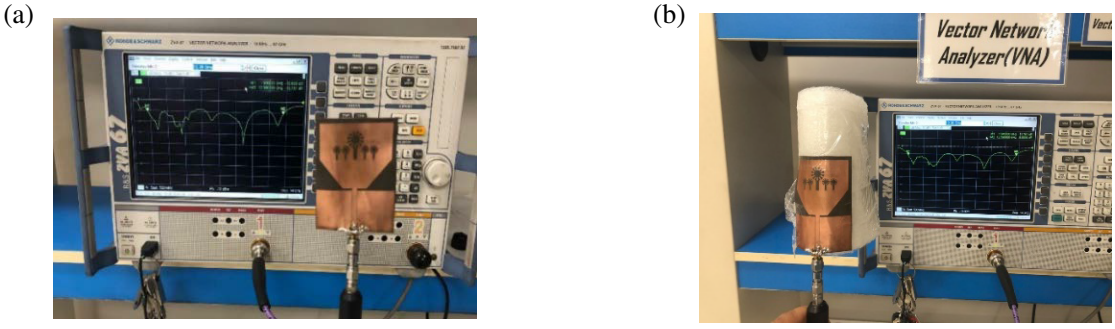

Figure 5. Measured reflection coefficient magnitude, $|S_{11}|$, (a) unbent proposed antenna, (b) proposed antenna under bending.

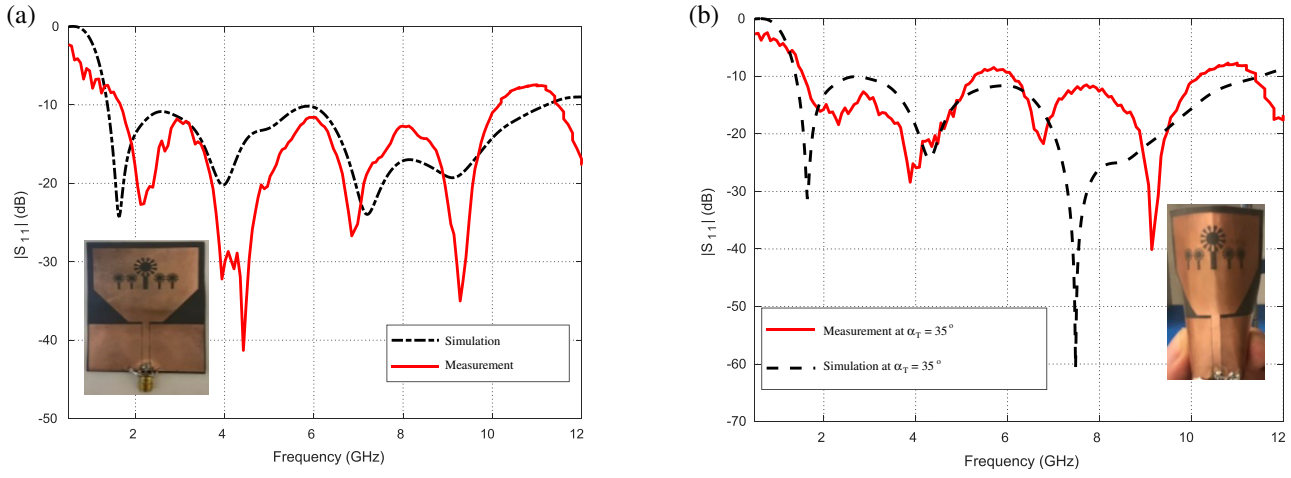

Figure 6. Comparison between the measured and simulated reflection coefficient for the designed and fabricated windmill-shaped fractals strip antenna (The inset shows a photograph of the fabricated prototype).

3.2. The Radiation Patterns Evaluation over the Frequency Band

The simulation-generated far-field patterns in the azimuth and elevation planes, specifically at $\phi = 0°$ and $\theta = 90°$ respectively, are illustrated in Figure 7. These patterns typically exhibit omnidirectional properties, barring instances when they are evaluated near the center frequencies of the impedance matching band. Across lower and higher frequencies within the operational range, the far-field patterns in the azimuth plane, $\phi = 0°$, tend to display almost circular symmetry as illustrated in Figure 7(a). In the elevation plane, $\theta = 90°$, the far-field patterns adopt the form of an 8-shaped figure, with the nulls of this figure positioned at the directions of $\phi = 90°$ and $\phi = 270°$. In Figure 7(b), slight deviations in the 8-shaped pattern arise due to additional nulls appearing at higher frequencies.

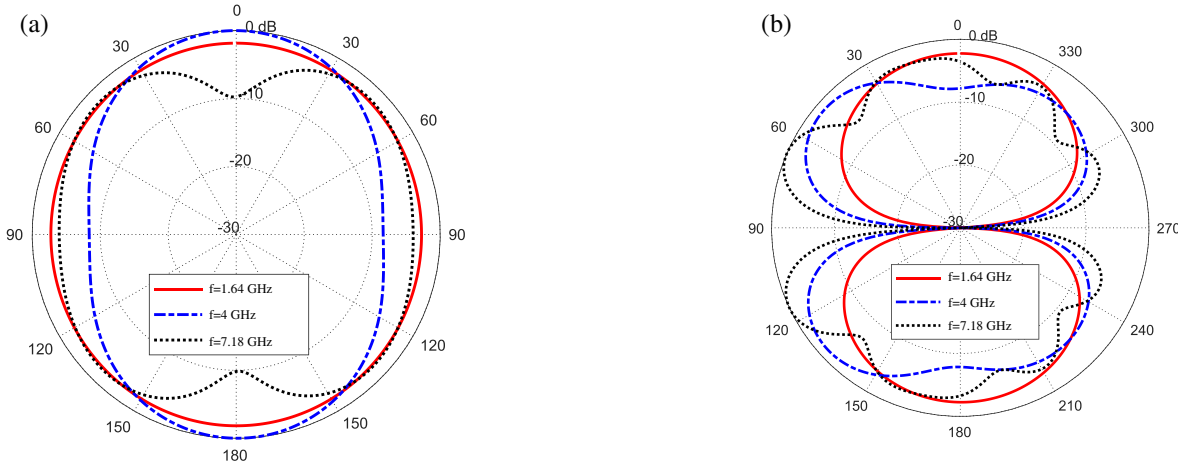

Figure 7. The far-field patterns of the windmill-shaped fractals strip printed antenna over the frequency band of operation in two mutually perpendicular planes, (a) azimuth plane $\phi = 0°$, and (b) elevation plane $\theta = 90°$.

To corroborate the simulated radiation patterns of the proposed antenna, they are cross-referenced with experimental measurements. In Figure 8, a comparison is illustrated between the far-field patterns obtained from experimental measurements at 6 GHz in the azimuth and elevation planes, $\phi = 0°$ and $\theta = 90°$, respectively, and those generated by the CST simulator. The experimental and simulated outcomes exhibit notable consistency, indicating a favorable alignment between them.

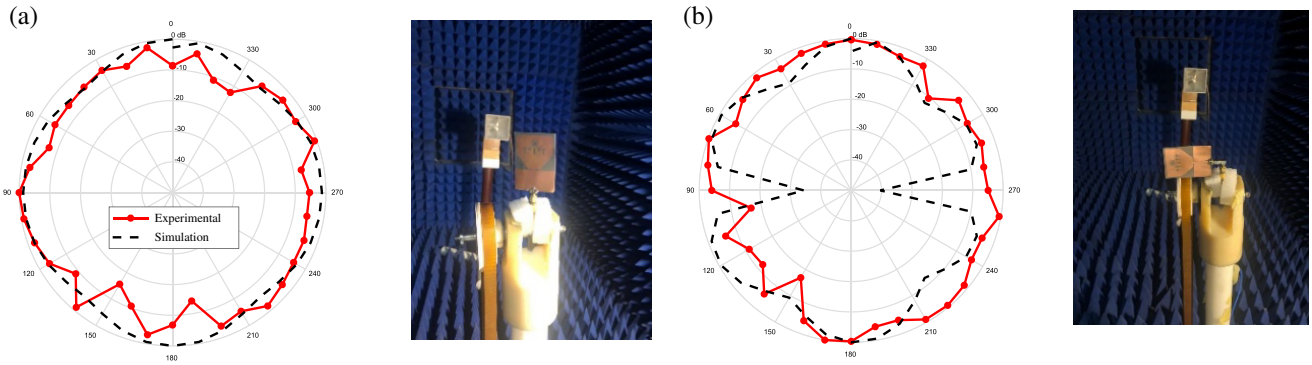

Figure 8. Comparison between measured radiation patterns of the proposed antenna at 6 GHz and corresponding simulation results in two mutually perpendicular planes, (a) azimuth plane $\phi = 0°$ and (b) elevation plane $\theta = 90°$ (Inset: Windmill-shaped fractal strip printed antenna within an anechoic chamber.).

3.3. Gain and Radiation Efficiency

The fluctuations in the maximum gain generated by the proposed antenna along with the corresponding radiation efficiency are assessed across the frequency span of 1 GHz to 12 GHz. As depicted in Figure 9, the graphical representation of the frequency-dependent performance of the maximum gain within the operational span is depicted. The maximum gain is within the range of 1.6 to 4.8 dBi throughout the frequency spectrum. Notably, a peak value approximately 4.8 dBi is observed specifically at 9 GHz.

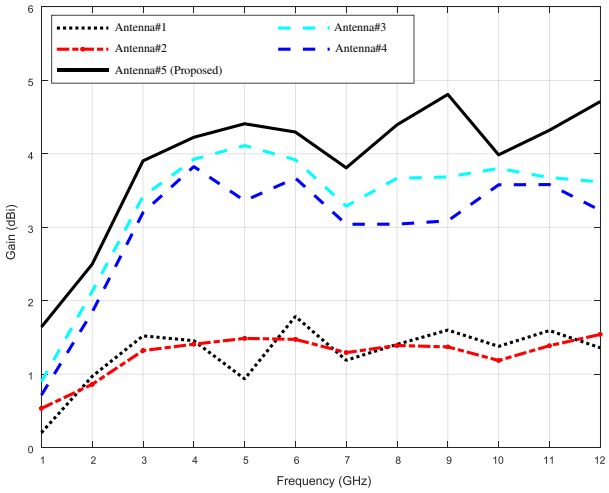

Figure 9. The changes in the antenna gain across the frequency range of 1–12 GHz at each of the five developmental stages.

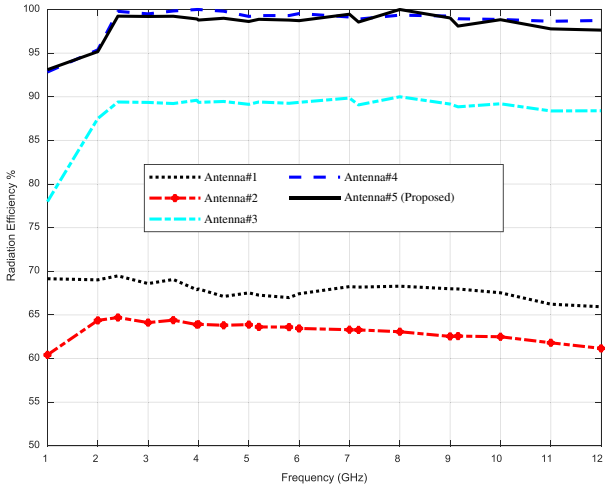

Figure 10. The fluctuations in antenna radiation efficiency over the 1–12 GHz frequency range at each of the five stages of development.

On the other hand, the behavior of radiation efficiency across the complete frequency range is illustrated in Figure 10. As indicated in the figure, the antenna exhibits impeccable radiation efficiency over the entire frequency span. The average radiation efficiency observed throughout the entire band is approximately 98%.

3.4. Surface Current Distribution

For operation across the ultra-wide frequency range of 1 GHz to 12 GHz, the antenna must exhibit diverse radiation mechanisms in order to encompass such ultra-wide spectrum of frequencies. Figures 11(a)

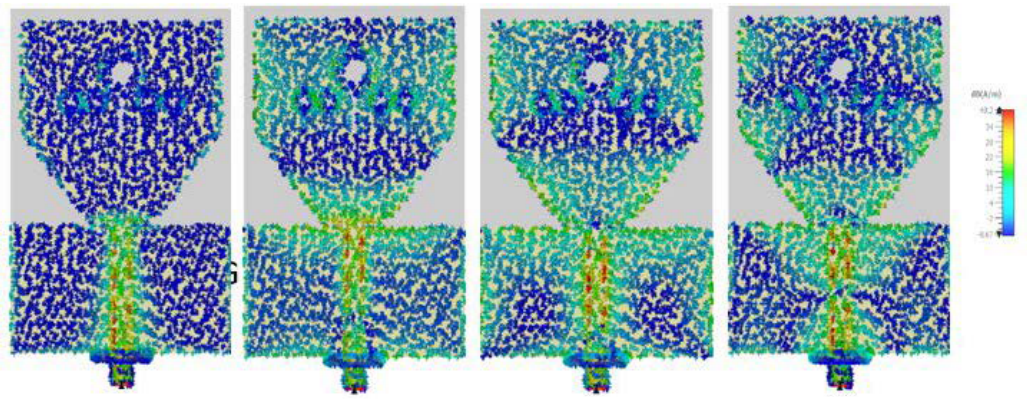

(a) (b) (c) (d)

Figure 11. The current distribution of the proposed antenna with ultra-wideband capabilities at the following frequencies: (a) 1.64 GHz, (b) 4 GHz, (c) 6 GHz, and (d) 9.17 GHz.

Table 2. Comparative evaluation of the proposed antenna performance with recently published antenna designs.

Work	Dimensions	Frequency Band (GHz)	% BW for Impedance Matching	Radiation Efficiency	Gain (dBi)	Substrate
[10]	$0.77\lambda_0 \times 0.77\lambda_0$	5.96–7.38	21.28%	NA	1.9–2.8	Rigid FR-4
[1]	$0.81\lambda_0 \times 1.15\lambda_0$	3.25–13	120%	NA	6.5	Flexible
[16]	$0.75\lambda_0 \times 1.00\lambda_0$	3–12	120%	80%	4	Flexible
[2]	$0.55\lambda_0 \times 0.69\lambda_0$	4.98–8.87	56.17%	NA	0.15–2.03	Rigid FR-4
[17]	$0.52\lambda_0 \times 0.77\lambda_0$	3.6–19.08	141.31%	NA	3	Flexible
[6]	$0.77\lambda_0 \times 0.91\lambda_0$	3.1–10.6	109.49%	92%	2–9	Rigid FR-4
[7]	$0.63\lambda_0 \times 0.78\lambda_0$	3–12.7	123.56%	NA	3.6	Rigid RT/Duroid 5880
[8]	$0.96\lambda_0 \times 1.35\lambda_0$	3.2–20	144.82%	NA	5.36	Rigid RT/Duroid 5880
[**Present**]	$1.05\lambda_0 \times 1.47\lambda_0$	1.37–11.25	156.6%	98%	4.8	Flexible

through 11(d) display the surface current distributions within the proposed antenna at frequencies of 1.64 GHz, 4 GHz, 6 GHz, and 9.15 GHz. The selection of these frequencies is guided by the resonance frequencies observed in the $|S_{11}|$ plot. The distribution of surface current is pervasive across the patch, feed line, and ground planes, and its configuration varies with changing frequencies.

Notably, as the frequency escalates, the appearance of higher-order modes becomes apparent, a phenomenon well-illustrated in Figure 11.

4. CONTRAST WITH THE PERFORMANCE OF OTHER PREVIOUSLY PUBLISHED DESIGNS

In order to underscore the value of our present research within the context of existing literature that shares similar objectives, we have included performance metrics for the proposed UWB flexible windmill-shaped fractal strip monopole antenna. These metrics are thoughtfully presented in Table 2, offering a comparison with a range of another fractal antenna designs recently introduced in the literature. Table 2 presents the diversity of antenna designs, encompassing both rigid and flexible models. The flexibility aspect is of paramount significance, given its relevance in applications involving flexible electronic devices and medical field. This flexibility equips the antenna to conform to non-planar surfaces and versatile configurations, which is particularly beneficial in healthcare applications.

As we delve into the comparison with the antennas featured in Table 2, our antenna design comes to the fore as an exceptional and one-of-a-kind solution. It boasts remarkable characteristics, including high gain, high radiation efficiency, flexibility, and operation with linear polarization, all over an exceptionally wide frequency range spanning from 1 to 12 GHz. This combination of features is paramount for achieving high data rates and enabling wideband communication, particularly in the context of on-body or in-body biosensor antennas. These biosensors, which are attached to or implanted within the human body, demand precise alignment and high-performance during communication. Our antenna's linear polarization capabilities facilitate this alignment seamlessly.

5. CONCLUSION

An innovative design for a windmill-shaped irregular hexagonal-monopole patch antenna has been introduced, intended for operation across ultra-wide frequency bands. Both simulation and experimental analysis confirm that the proposed antenna spans a frequency range from 1 to 12 GHz. The antenna has been implemented on a flexible substrate with a thickness measuring 0.2 mm. The antenna's bandwidth is enhanced by integrating five windmill strips, arranged into irregular hexagonal shapes, combined to establish the monopole patch configuration. A coplanar waveguide (CPW) structure serves as the feeding mechanism, allowing the complete antenna structure, including the feeding line, to be confined to one side of the dielectric substrate while leaving the other side unoccupied. A physical prototype of the

antenna has been manufactured for experimental validation. The antenna exhibits a remarkable 156.6% bandwidth and an impressive bandwidth-dimension ratio of 4457. Moreover, the radiation efficiency is consistently maintained above 98% across the entire bandwidth (1–12 GHz).

ACKNOWLEDGMENT

The authors would like to acknowledge the support provided by Researchers Supporting Project number (RSPD2023R868), King Saud University, Riyadh, Saudi Arabia.

REFERENCES

1. Lakrit, S., S. Das, B. T. P. Madhav, and K. Vasu Babu, "An octagonal star shaped flexible UWB antenna with band-notched characteristics for WLAN applications," *Journal of Instrumentation*, Vol. 15, No. 2, P02021, 2020.
2. Sharma, N. and S. S. Bhatia, "Stubs and slits loaded partial ground plane inspired novel hexagonal ring-shaped fractal antenna for 5G/LTE/RFID/GSM/Bluetooth/WLAN/WiMAX wireless applications: Design and measurement," *Progress In Electromagnetics Research C*, Vol. 112, 99–111, 2021.
3. Ouf, E. G. E., M. A. E. Abo-Elhassan, A. E. Farahat, K. F. A. Hussein, and S. Mohassieb, "High performance two-arm antenna for super wideband operation," *Progress In Electromagnetics Research C*, Vol. 125, 105–115, 2022.
4. Mandelbrot, B. B., *Fractals: Form, Chance and Dimension*, W. H. Freeman, 1977, ISBN 0-7167-0473-0.
5. Anguera, J., A. Andújar, J. Jayasinghe, V. V. S. S. S. Chakravarthy, P. S. R. Chowdary, J. L. Pijoan, T. Ali, and C. Cattani, "Fractal antennas: An historical perspective," *Fractal and Fract.*, Vol. 4, 3, 2020.
6. Marzouk, M., Y. Rhazi, I. H. Nejdi, F.-E. Zerrad, M. Saih, S. Ahmad, A. Ghaffar, and M. Hussein, "Ultra-wideband compact fractal antenna for WiMAX, WLAN, C and X band applications," *Sensors*, Vol. 23, 4254, 2023.
7. Khan, M. A., U. Rafique, H. Ş. Savci, A. N. Nordin, S. H. Kiani, and S. M. Abbas, "Ultra-wideband pentagonal fractal antenna with stable radiation characteristics for microwave imaging applications," *Electronics*, Vol. 11, 2061, 2022.
8. Saleem, I., U. Rafique, S. Agarwal, H. S. Savci, S. M. Abbas, and S. Mukhopadhyay, "Ultra-wideband fractal ring antenna for biomedical applications," *International Journal of Antennas and Propagation*, Vol. 2023, Article ID 5515263, 9 pages, 2023.
9. Kaur, N., J. Singh, and M. Kumar, "Hexagonal ring-shaped dual band antenna using staircase fractal geometry for wireless applications," *Wireless Pers. Commun.*, Vol. 113, 2067–2078, 2020.
10. Reha, A., A. El Amri, O. Benhmammouch, A. O. Said, A. El Ouadih, and M. Bouchouirbat, "CPW-fed H-tree fractal antenna for WLAN, WIMAX, RFID, C-band, HiperLAN, and UWB applications," *Int. J. Microw. Wirel. Technol.*, Vol. 8, 327–334, 2016.
11. Daniel, R. S. and R. Selvaraj, "A low-profile split ring monopole antenna loaded with hexagonal split ring resonator for RFID applications," *Progress In Electromagnetics Research M*, Vol. 92, 169–179, 2020.
12. Regulagadda, N. R. and U. V. R. Kumari, "A multiband flexible wideband CPW wearable slot antenna for biomedical and IoT applications," *Progress In Electromagnetics Research C*, Vol. 135, 131–144, 2023.
13. Amsaveni, A. and M. Bharathi, "Design and implementation of H-shaped fractal antenna for UWB applications," *2021 International Conference on Advancements in Electrical, Electronics, Communication, Computing and Automation (ICAECA)*, 1–5, Coimbatore, India, 2021.
14. Muthu, R. C. and R. B. Rani, "Asymmetric CPW-fed hexagonal monopole antenna with Boomerang-shaped fractals for ultra-wideband applications," *Frequenz*, Vol. 76, Nos. 9–10, 555–568, 2022.

15. Sediq, H. T., J. Nourinia, C. Ghobadi, and B. Mohammadi, "A novel shaped ultrawideband fractal antenna for medical purposes," *Biomedical Signal Processing and Control*, Vol. 80, Part 2, 2023.
16. Sun, Y., T. I. Yuk, and S. W. Cheung, "Design of a textile ultra-wideband antenna with stable performance for body-centric wireless communications," *IET Microw. Antennas Propag.*, Vol. 8, 1363, 2014.
17. Zou, Q. and S. Jiang, "A compact flexible fractal ultra-wideband antenna with band notch characteristic," *Microwave and Optical Technology Letters*, Vol. 63, No. 3, 895–901, 2021.
18. Awan, W. A., N. Hussain, and T. T. Le, "Ultra-thin flexible fractal antenna for 2.45 GHz application with wideband harmonic rejection," *AEU — International Journal of Electronics and Communications*, Vol. 110, 2019.
19. Fahmy, W. M., A. E. Farahat, K. F. A. Hussein, and A. A. Ammar, "High Q-factor bandstop filter based on CPW resonator broadside-coupled to CPW through-line," *Progress In Electromagnetics Research B*, Vol. 86, 121–138, 2020.
20. Fahmy, W. M., A. E. Farahat, K. F. A. Hussein, and A. A. Ammar, "Dual-band bandpass filter optimized for high Q-factor," *Appl. Comput. Electromagn. Soc. J. (ACES)*, Vol. 36, 398–410, 2021.